The Consequences of Interface Mixing on Organic Photovoltaic Device Characteristics

By David M. Huang[b], Scott A. Mauger[a], Stephan Friedrich[c], Simon J. George[d], Daniela Dumitriu-LaGrange[a], Sook Yoon[a], and Adam J. Moulé[a*]

[a] Prof. A. J. Moulé, Scott A. Mauger, Dr. D. D. LaGrange, Dr. Sook Yoon
Chemical Engineering and Materials Science Department
University of California, Davis, CA 95616, USA
E-mail: amoule@ucdavis.edu
[b] Dr. David M. Huang
School of Chemistry & Physics
The University of Adelaide
SA 5005, Australia
[c] Dr. Stephan Friedrich
Lawrence Livermore National Laboratory
7000 East Ave., L-188
Livermore, CA 94550, USA
[d] Dr. Simon J. George
Advanced Biological and Environmental X-ray Facility
Lawrence Berkeley National Lab
1 Cyclotron Road Mail Stop 6R2100
Berkeley, CA 94720, USA
[*] Prof. A. J. Moulé - To whom correspondence should be addressed
Keywords: Photovoltaic Devices, Solar Cells, Conducting Polymers, Organic Electronics, Charge Transport

Abstract

Organic bulk-heterojunction solar cells are being developed as a low-cost alternative to inorganic photovoltaics. A key step to producing high-efficiency bulk-heterojunction devices is film curing using either heat or a solvent atmosphere. All of the literature examining the curing process have assumed that improvement of the bulk-heterojunction morphology is the reason for the increased filling factor, short-circuit current density, and efficiency following heat or solvent treatment. We show in this article that heat treatment causes the donor polymer (P3HT) and polymer electrode (PEDOT:PSS) to mix physically to form an interface layer. This interface layer is composed of a mixture of P3HT and PSS in which the P3HT is oxidized to $P3HT^{+}$. This mixed layer affects the open-circuit voltage and compensation voltage by limiting the dark current. This result implies that a simplistic description of the P3HT/PEDOT:PSS contact as a sharp interface between bulk P3HT and bulk PEDOT:PSS cannot adequately capture its electrical characteristics.

1 Introduction

The study of organic photovoltaic (OPV) materials and devices is a rapidly growing scientific field that is gaining increasing technological relevance. A recent NREL cerified power conversion efficiency (PCE) record of 8.13% was reported in 2010.[1] Efficiency records such as these show that OPV technology is increasingly capable of competing with other thin-film PV technologies. However, many questions about basic device physics still persist.

Polymer-based solar cells consist of several polymer, copolymer, and mixed polymer/fullerene layers with thicknesses less than 100 nm, as shown in Figure 1. Since the layers are so thin, the properties of the interfaces dominate the electrical function of the layers. For this reason, an understanding of the interface morphologies of the polymers used in these devices is needed. There are two types of interfaces in a bulk-heterojunction (BHJ) OPV device. First and most studied are the interfaces between the donor and acceptor materials in the BHJ layer. The mixture of poly(3-hexylthiophene) (P3HT) and [6,6]-phenyl-C_{61}-butyric acid methyl ester (PCBM) is the most studied BHJ layer material. One of the main concerns in recent years has been control of the layer morphology in bulk-heterojunction (BHJ) mixtures of donor polymers with fullerene acceptors. It has been shown that the use of thermal treatment, solvent soaking, or solvent additives can greatly improve the PCE by curing the BHJ morphology.[2–4] For a BHJ layer composed of P3HT mixed with PCBM, curing the BHJ layer results in increased domain size, hole mobility, and crystallinity of the P3HT.[5–7] All articles describing the effects of curing the morphology have assumed that changes to the BHJ morphology and resulting electronic changes are the sole reason for changes to device properties.

The second type of interface is that between material layers, such as electrode and BHJ layers and it is this type of interface that will be the focus of this article. The BHJ layer is typically coated onto a substrate of indium-tin oxide with a thin layer of poly(3,4-ethylenedioxythiophene):poly(styrenesulfonate)) (PEDOT:PSS) on top. PEDOT:PSS is used as the polymer anode in virtually all organic light-emitting diodes (OLEDs) and organic photovoltaics (OPV). This electrode material is so widely used because it is insoluble in organic solvents, has a well-defined work function (Φ) of around 5.1 eV,[8] is a

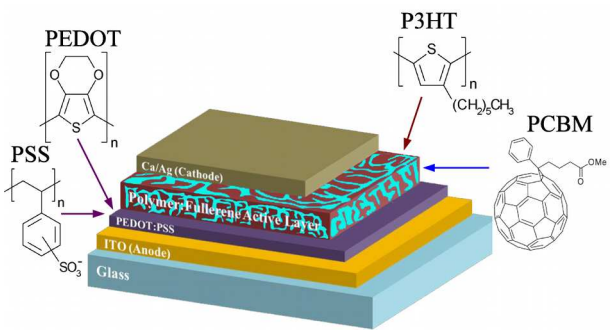

Figure 1: Schematic of a typical polymer solar cell with (from top to bottom) a Ca/Ag cathode, a polymer:fullerene active layer consisting of a mixture of P3HT (electron donor) and PCBM (electron acceptor), a PEDOT:PSS hole-transporting layer, and an ITO anode on a glass substrate.

hole conductor, and forms an ionomer, so the dopant PSS^- does not separate from the PEDOT matrix due to Coulombic attraction.[9] There is experimental evidence that, when spin coated in air, PSS and PEDOT forms vertically segregated layers with PSS at the top surface.[8] Further research in this area has shown that PEDOT:PSS microdomains form that are rich in PEDOT near the center and have little PEDOT at the surface. Upon heating, the PEDOT-rich domains form lateral (in plane) domains that are much more higly conductive than perpendicular to the film surface.[10–12]

Several organic or inorganic material have been investigated for use as "hole only" replacements for PEDOT:PSS.[13] The desired properties for this layer are an Ohmic contact to the HOMO of the donor polymer in the BHJ layer, optical transparancy, ease of preparation and deposition, and selectivity to hole transport, which can also be written as electron blocking. The use of a PEDOT:PSS replacement anode composed of a blend of 4,4'-bis[(p-trichlorosilylpropylphenyl)-phenylamino]biphenyl ($TPDSi_2$) poly[9,9-dioctylfluorene-co-N-[4-(3-methlypropyl)]-diphenylamine (TFB) has also been shown to offer greater hole selectivity than PEDOT:PSS.[14] The group of Karl Leo has published a number of articles that detail the increase in electrode selectivity for mixtures of evaporated hole transport materials that form doped hole selective layers.[15, 16] $V2O_5$ and NiO have also been investigated for use as PEDOT:PSS replacement electrodes.[17–19] Although isolated results have been published using these other electrode materials, PEDOT:PSS was used as the anode material for all verified device records.

PEDOT:PSS is considered metallic because it has a continuous density of the states at the Fermi level.[20, 21] Unlike a typical metal, PEDOT:PSS does not have a large free electron density and so the Φ on PEDOT:PSS does not change greatly with contact to other materials, i.e. large dipole layers do not form.[22, 23] One interesting phenomenon with BHJ OPV devices on PEDOT:PSS layers is that the PEDOT:PSS is able to accept holes from nearly any polymer, regardless of the highest occupied molecular orbital (HOMO) level of the polymer. Scharber et. al. showe that the open circuit voltage (V_{oc}) of BHJ OPV devices depends only on the energy gap between the HOMO of the polymer and the lowest unoccupied molecular orbital (LUMO) of the fullerene.[24] In organic light emitting diodes (OLEDs) a barrier for hole injection from the PEDOT:PSS into a polymer layer is a well-established phenomenon.[25] Recent work using ultraviolet photoelectron spectroscopy has shown that the barrier for hole injection into PEDOT:PSS is lower than expected in some devices.[26] For an OPV device in which P3HT with a Φ of 4.7 eV has to inject a hole into PEDOT:PSS with a Φ of 5.1 eV the contact appears to be Ohmic and no net energy loss occurs. It has been suggested that either the orientation of the polymer at the interface or the formation of a surface dipole layer could change the injection barrier.[27, 28]

We show in this article that the V_{oc} also depends on the degree of mixing between PEDOT:PSS and the BHJ polymer. We also show that upon heating, P3HT in the mixed layer is oxidized to $P3HT^+$ by reaction with HPSS at the anode/BHJ interface. This electrochemical reaction increases the selectivity for hole transport of the cathode and ultimately leads to an increased device PCE. Thus, we show that thermal treatment not only impacts performance through its effect on the BHJ morphology, as is traditionally assumed, but also through its effect on the anode/BHJ interface.

2 Results and Discussion

In the following sections, we use contact angle (θ_c) measurements, X-ray absorption near edge structure (XANES), and neutron reflectometry (NR) to show that P3HT physically mixes with PEDOT:PSS upon heating. Then we use UV/VIS/NIR and FTIR spectroscopy to show that P3HT is oxidized to $P3HT^+$ in the mixed layer by reaction with excess HPSS. Finally we use Kelvin force probe and current density – voltage (J–V) measurements to show that formation of this mixed interface layer increases the V_{oc} of OPV devices. A complete analysis of the J–V data is in preparation for a separate publication.

The focus of this article is structural and chemical changes at the active layer/PEDOT:PSS interface. Rather than characterize the structure of complete devices, we focus on the P3HT/PEDOT:PSS interface by preparing samples comprising a layer of P3HT deposited on a layer of PEDOT:PSS on glass or silicon substrates. Mixtures of P3HT/PCBM or pure P3HT on PEDOT:PSS gave identical results for all of the tests relating to formation of the interface layer, so for simplicity, only the results for pure P3HT will be listed. Samples were subjected to different heat-treatment temperatures and washed repeatedly with chlorobenzene (CB), in which P3HT is soluble, in order to

determine whether any sort of physical or chemical bonding between P3HT and PEDOT:PSS takes place upon heat treatment. The formation of a mixed interface layer has been previously studied with much less detail for hole injection layers on PEDOT:PSS surfaces for OLED applications.[29]

2.1 Layer Mixing

The large difference between the hydrophobicities of P3HT and PEDOT:PSS makes contact angle (θ_c) measurements a sensitive probe of the presence of these materials at a surface that may consist of one or both of these two components. To confirm the presence of an interlayer at the PEDOT:PSS/bulk-heterojunction interface, a series of bilayer samples were fabricated. These samples were heated to various temperatures and then the P3HT was washed off using CB. Figure 2 shows the θ_c of a water droplet on films of PEDOT:PSS, P3HT on PEDOT:PSS, and P3HT on PEDOT:PSS washed with CB after heat treatment, versus the heat-treatment temperature. As shown in Figure 2, the θ_c of P3HT (i.e. P3HT on PEDOT:PSS) is the same (107°) for heat treatment at room temperature and 180°C. This θ_c was therefore assumed to be constant over the temperature range studied. On the other hand, the θ_c of PEDOT:PSS decreases slightly from 15° to 5° with increasing heat treatment temperature from room temperature to 180°C. This behavior could be due to an increasing predominance of the more hydrophilic PSS at the surface as a result of thermal annealing. For the heat-treated samples with P3HT on PEDOT:PSS washed with CB, θ_c shows a distinct transition around 150°C from a θ_c similar to that of PEDOT:PSS to one resembling that of P3HT, indicating the presence of a P3HT surface layer for the washed samples heated above 150°C.

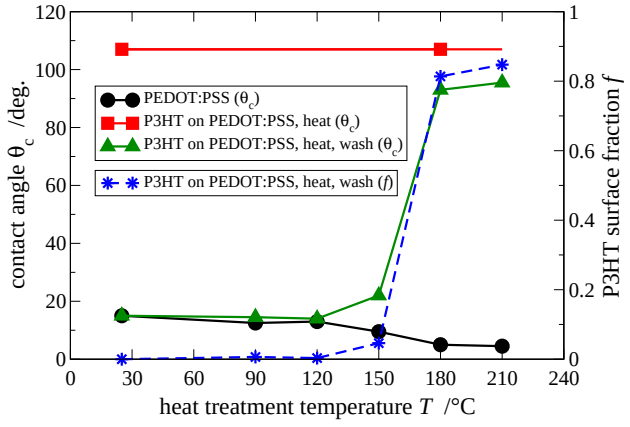

Figure 2: Contact angle (measured at room temperature) of a water droplet on films of PEDOT:PSS, P3HT on PEDOT:PSS, and P3HT on PEDOT:PSS washed with chlorobenzene after heat treatment vs heat-treatment temperature. Also shown is the fraction f of the surface covered by P3HT on the washed samples estimated from Equation (1).[30]

To quantify the presence of P3HT at the interface, the fraction f of the surface covered by P3HT on the washed samples was calculated at each temperature T using the Cassie–Baxter equation [30],

$$\cos\theta_c = f\cos\theta_{P3HT} + (1-f)\cos\theta_{PEDOT:PSS}\,, \qquad (1)$$

where θ_{P3HT} and $\theta_{PEDOT:PSS}$ are the measured contact angles of water on P3HT and PEDOT:PSS respectively (assuming that θ_{P3HT} is the same at all temperatures). The surface coverage of P3HT on washed samples was calculated to increase from 0 to ∼5% at 150°C and then to jump to over 80% at 180°C and above, as shown in Figure 2. This result indicates an almost monolayer coverage at these high temperatures and clearly demonstrates that P3HT is tightly bound (either physically or chemically) to PEDOT:PSS upon heating to temperatures of 150°C and above, indicating the formation of an intermixed layer between the two materials. Similar θ_c experiments performed with PCBM on PEDOT:PSS showed that PCBM does not form an interlayer with PEDOT:PSS, since the contact angle was identical for PEDOT:PSS and for PEDOT:PSS that had PCBM spin-coated then washed off of it.

We used X-ray absorption spectroscopy to determine the chemical composition of the mixed layer because it is a sensitive technique to measure the element-specific bonding structure. For samples much thicker than the X-ray absorption length, the absorption can be recorded by monitoring either the total electron yield (TEY) or the partial fluorescence yield (PFY) emitted from the sample in response to the core hole excitation. Since the electron escape depth of several nm is much shorter than the 1 μm escape depth for soft X-rays, TEY measurements of the X-ray absorption provide information on surface chemistry, while PFY measurements provide complementary information about bulk chemistry.

We have taken X-ray absorption spectra of PEDOT:PSS and P3HT samples, with and without P3HT on top, before and after heating, on the carbon K absorption edge. Figure 3 shows the surface-sensitive TEY data, while the PFY data are shown in the supporting material in Figure S1. The TEY spectra show five peaks that have been assigned as follows: 283.6 eV to the π^* transition of carbon reduced by either Na^+ or H^+, 284.8 eV to the π^* transition that corresponds to aromatic carbon and is broadened by the C–S bond,[31, 32] 287 eV to the C–H bonds associated with the alkane chain[31] with possible contributions from the C–O bonding group[32], 288.2 eV to the π^* transition from C–H bonds associated with an aromatic ring [31], and finally transitions >290 eV to σ^* transitions.

To differentiate between signals coming from the PEDOT and PSS polymers, we compared samples of Na^+PSS^- to untreated PEDOT:PSS and heated PEDOT:PSS films. The Na^+PSS^- spectrum has strong features at 284.7 eV and 288.5 eV which indicate the presence of aromatic carbon and aromatic carbon hydrogen bonds, respectively. While all samples will have aromatic carbon, only PSS has a lot of C–H bonds to aromatic carbons. The heated PEDOT:PSS film also has

higher intensity features at 284.7 eV and 288.5 eV than the unheated PEDOT:PSS sample. We take this as confirmation of previously reported data that shows that upon heating, the PSS moiety moves to the sample surface.[8] Supporting this conclusion is a reduction of intensity for the 287 eV peak for heated PEDOT:PSS, which indicates reduced C–O bond and C–H (non-aromatic) character at the surface, indicating the absence of PEDOT. A XANES spectrum of P3HT (dotted line) shows greatly reduced intensity for the π^* peak at 284.7 eV and a high-intensity peak at 287 eV indicating the presence of alkane chains. There is no discernable peak at 288.5 eV.

Next a sample of PEDOT:PSS that had P3HT washed off after heating to a temperature of 150°C was measured. For simplicity, this sample will be refered to as "washed". The washed sample shows peak intensity both at 287 eV and 288.5 eV. Since the 287 eV peak is associated with P3HT alkane chains and the 288.5 eV peak with the aromatic C–H bonds of PSS, it can be concluded that both P3HT and PSS are present in the top several nm of the sample surface. The peak at 284.7 eV is larger in the washed sample than for either the unheated PEDOT:PSS or P3HT. This is further confirmation of increased PSS as the surface.

The washed data was fit by numerically averaging the Na^+PSS^- and pure P3HT spectra with a 6:5 ratio. Note that this data cannot be directly compared to the surface coverage calculated using the Cassie-Baxter equation and θ_c data because the XANES experiment has a sensitivity to a greater penetration depth at the sample surface. The fit spectra exactly reproduce the line shape and suggest that only P3HT and PSS are present at the surface and that PEDOT is not within several nm of the surface. That a numerical average of two separate spectra can be used to reproduce the washed-sample data indicates that the PSS and P3HT are forming a mixed layer. It also indicates that the bonding structure of both polymers remains intact. There is no indication of bond breaking or bond formation between PSS and P3HT. A change in bonding structure would cause a shift of electron density around the atoms and therefore a shift in the XANES spectrum or formation of new peaks.

The PFY spectra (Supporting Information Figure S1) show nearly identical spectra for PEDOT:PSS with and without heating and P3HT washing. This indicates that the change in the surface has very little effect on the bulk of the film.

Neutron reflectivity measurements provide information of film composition as a function of depth. Neutron reflectivity data for selected samples are shown in Figure 4a, along with fits to the data using a slab model for the scattering length density (SLD) profile of the film. The SLD profiles near the top (air) interface obtained from the model fitting are shown in Figure 4b for selected samples. (The neutron reflectivity data and fits and modeled SLD distributions for all measured samples are given in Figures S2 and S3, respectively, of the Supporting Information.) The SLDs of PEDOT:PSS, $\rho_{PEDOT:PSS}$, and P3HT, ρ_{P3HT}, were obtained from the fits of the neutron reflectivity data for

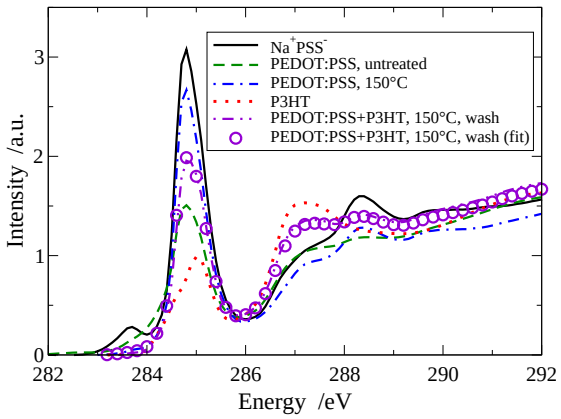

Figure 3: X-ray absorption near edge structure (XANES) spectra of the carbon K edge of Na^+PSS^-, untreated PEDOT:PSS, PEDOT:PSS heated to 150°C, P3HT, and P3HT on PEDOT:PSS that was heated to 150°C and then washed with chlorobenzene. The points are a numerical average of the curves for the heated PEDOT:PSS film and the P3HT film with a weighting of 6:5.

the samples with only PEDOT:PSS and only P3HT, respectively, on silicon. The values of $\rho_{PEDOT:PSS} = 1.80 \times 10^{-6}$ Å^{-2} and $\rho_{P3HT} = 0.786 \times 10^{-6}$ Å^{-2} are consistent with those calculated using the NIST SLD Calculator[33] from the molecular formulas of PEDOT, PSS, and P3HT and approximate densities of 1.1 g/cm^3 for these polymers of 1.68×10^{-6} Å^{-2} (assuming a 1:6 mixture of PEDOT and PSS with SLDs of 1.85×10^{-6} Å^{-2} and 1.49×10^{-6} Å^{-2}) and 0.68×10^{-6} Å^{-2}, respectively.

Figure 4b shows that SLD profiles of the untreated PEDOT:PSS film and the film in which P3HT was spin-coated on to PEDOT:PSS and then washed with CB without heat treatment are virtually indistinguishable, indicating the absence of P3HT on the latter film, which is consistent with θ_c and XANES results. For the films that were heat treated after deposition of P3HT on to PEDOT:PSS but before washing with CB, the interface width (twice the "roughness" σ) is larger than that of the untreated PEDOT:PSS film and increases with temperature, from 3.4 nm for the film heated to 150°C to 6.4 nm and 7.0 nm respectively for the films heated to 180°C and 210°. The increased interface width could be due to (1) increased roughness of the interface, (2) vertical segregation of PSS and PEDOT (with PSS nearer the surface), or (3) the presence of P3HT on the surface, which could also be intermixed with PEDOT and PSS. Unfortunately, the ordering of the magnitudes of the SLDs, $\rho_{P3HT} < \rho_{PSS} < \rho_{PEDOT}$, makes it difficult to distinguish between these three cases. However, the absence of an increase in the measured surface roughness measured by AFM with heat treatment (not shown) allows us to rule out case (1). We also find that the fit to the neutron reflectivity data for the 210°C-

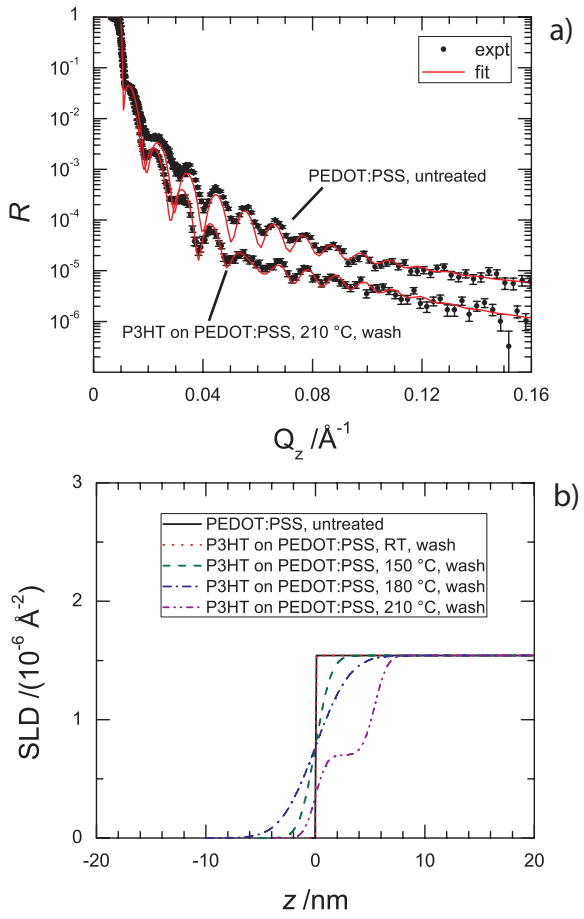

Figure 4: (a) Neutron reflectivity data and model fits for an untreated PEDOT:PSS film and for P3HT on PEDOT:PSS heated to 210°C then washed with chlorobenzene (both on silicon wafer substrates). (b) Scattering length density (SLD) profiles vs distance from the top surface of the film from fits to reflectivity data for untreated PEDOT:PSS, unannealed P3HT on PEDOT:PSS washed with chlorobenzene, and heat-treated P3HT on PEDOT:PSS washed with chlorobenzene, heated to 150°C, 180°C, and 210°C. Only the region close to the top (air) interface is shown.

heated film is noticeably improved when a several-nanometer layer of P3HT is assumed to exist on top of the PEDOT:PSS layer (as shown in Figure 4) instead of simply assuming a rough PEDOT:PSS interface. The 150°C- and 180°C-heated samples do not seem do have a distinct P3HT layer, but a thin layer with lower SLD is clearly present. When analyzed in the context of the other measurements, the neutron reflectivity results indicate that the bi-layer samples heated above 150°C form a few nanometers of P3HT intermixed PEDOT:PSS, with a predominance of PSS over PEDOT near the interface. After washing with a good solvent for P3HT this intermixed layer remains. The neutron reflectivity results also show that heating to higher temperatures increases the thickness of the intermixed layer.

2.2 Mixing Mechanism

We showed in section 2.1 that with heating, P3HT mixes with PEDOT:PSS at the interface and that the PEDOT:PSS vertically segregates so that the interface layer is composed almost entirely of PSS and P3HT. Further, we showed that the P3HT in this layer becomes insoluble. There are three mechanisms that can be imagined to explain the formation of this insoluble P3HT/PSS layer:

1. P3HT chemically reacts with PSS upon heating leading to the breaking of some conjugated bonds and the formation of new P3HT/PSS chemical bonds;

2. P3HT physically mixes with PSS upon heating and becomes trapped in a mixed layer, but remains uncharged;

3. P3HT physically mixes with PSS upon heating and electrochemically reacts to form $P3HT^+$ and PSS^-.

Mechanism (1) is unlikely because there is no evidence of the formation of new bond types in the XANES data (Figure 3). We further tested whether new bonds form by comparing FTIR plots (Supporting Information Figure S4) of ground powder mixtures of PEDOT:PSS and P3HT before and after heating to 180°C for one hour. Comparison of the two spectra show essentially identical peak ratios for all bond types. We expect that the most likely possible reaction is an acidic attack of the thiophene ring of P3HT by the HSO_3 group of PSS. If this reaction occured a new peak at 2535 cm^{-1} would appear for a S–H bond.[34] Since this peak is absent, we conclude that no bond forming or bond breaking reaction occurs between P3HT and PSS upon heating.

Mechanism (2) and (3) can be distinguished by whether the P3HT becomes oxidized by the PSS or whether it is simple mixing of neutral species. Presented in Figure 5 are UV/VIS/NIR difference spectra for a PEDOT:PSS/P3HT film that has been treated to increasing heating temperatures. Figure 5a shows the spectra of the heated films subtracted by the spectrum of the room temperature (RT) film in the visible and Figure. 5b shows the same data on a different scale in the near infrared (NIR). The spectra are displayed in this manner because separate diffraction gratings are required to cover the two measurement ranges and because $P3HT^+$ has a much lower absorbance than P3HT.

Figure 5a (visible wavelengths) shows that mild heating (up to 120°C) increases the P3HT absorption, probably due to increased ordering in the film.[35] However at higher temperatures, visible absorption increasingly bleaches. Figure 5b (NIR) shows the growth of an absorption peak centered at $\sim$ 900 nm.[36] This NIR peak has been assigned previously to $P3HT^+$.[37, 38] The fact that $P3HT^+$ is formed with increased

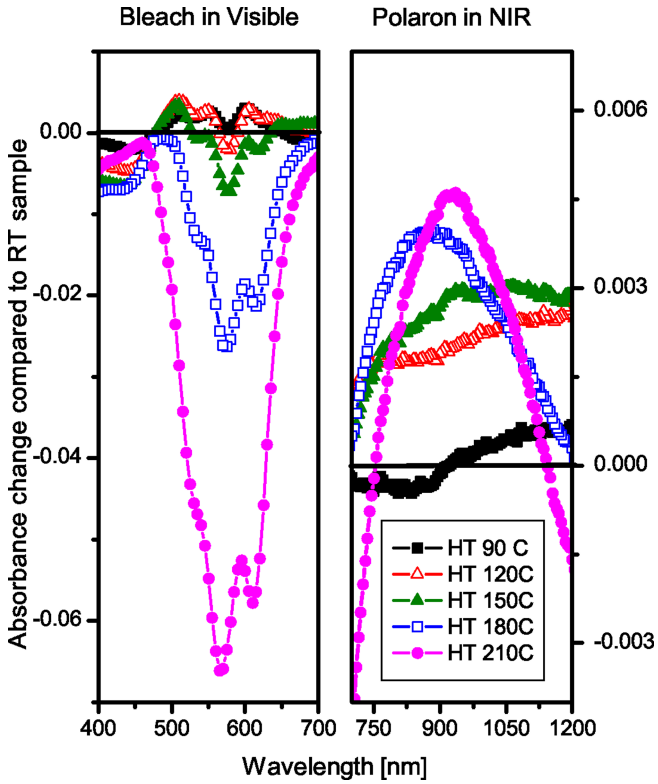

Figure 5: UV/VIS/NIR difference spectra of bi-layer samples of PEDOT:PSS/P3HT heated to 90°C, 120°C, 150°C, 180°C, and 210°C.

heating is proof that the mixing is accompanied by oxidation of P3HT in the mixed layer. The PEDOT:PSS used for hole-only layers in OPV devices has a PEDOT:PSS ratio of 1:6. The much larger PSS content means that most of the PSS is present as either HPSS or Na^+PSS^-. Earlier work showed that both HPSS and NaPSS are present in commercial solutions of PEDOT:PSS with NaPSS being the minority product.[8] We assign the following mechanism for the oxidation of P3HT:

$$2\ \mathrm{P3HT} + 2\ \mathrm{HPSS} \rightleftarrows 2\ \mathrm{P3HT^+} + 2\ \mathrm{PSS^-} + \mathrm{H_2}\,, \qquad (2)$$

This mechanism indicates that the P3HT is oxidized by HPSS to $P3HT^+$ and HPSS is reduced to PSS^-, which makes sense considering that the proton is very loosely bound in HPSS, which has a pKa of 1.2. We verified this mechanism by mechanically mixing a pellet of powdered HPSS and P3HT in a sealed container and then heating to 180°C for 10 min and then injecting the gas above the pellet into a gas chromatograph mass spectrometer (GCMS). As seen in Figure S5 in the Supporting Information, H_2 is detected in the case where P3HT and HPSS are heated. This is most likely a multi-step reaction, the details of which are beyond the scope of this publication.

Since we see no clear difference in the FTIR spectrum, we believe that only a fraction of the HPSS in the thin mixed layer is reduced. We are not able to quantify the extent of the electrochemical reaction from the NIR spectra in Figure 5b because the (1) conjugation length of P3HT, (2) the mixing ratio of the PSS and P3HT, (3) the exact thickness of the intermixed layer, and (4) the absorption coefficient of $P3HT^+$ cannot be measured to sufficient accuracy. The bleaching of P3HT in Figure 5a cannot be used to determine the reaction extent because the intermixed layer represents such a small fraction of the total absorbance and some absorbance change also occurs due to changes in the BHJ morphology.

2.3 Electrical Effects of Interlayer Formation

Both HPSS and PSS^- are unconjugated and so do not transport charges. This means that the oxidized P3HT at the interface is the only charge carrier. The presence of an oxidized P3HT layer suggests the Fermi level in the intermixed layer is much closer to the HOMO of P3HT than the LUMO. We used Kelvin force probe measurements to determine the Fermi level at the interface and then current-voltage measurements to determine the effect that this electronic change has on the OPV device performance.

Kelvin force probe measurements make a direct measurement of the Fermi energy of a surface.[39] The work function (Φ) of the surface, defined as the minimum energy required to remove an electron from the surface.[40] We prepared two sets of PEDOT:PSS samples with and without P3HT coated on top. The samples were heated at temperatures ranging from room temparature to 210°C for 5 minutes. The samples were then all washed multiple times with CB. Then the Fermi energy of the samples was measured. The samples that were pure PEDOT:PSS all have continuous and partially filled density of states (DOS) at the Fermi energy, so Φ is directly measured and shows values near the literature reported value of -5.2 eV (Figure 6). Φ increases slightly with increasing heat treatment, which means that more PSS on the surface makes it more difficult to remove an electron from the surface. For the P3HT washed samples, the measured Fermi energy decreases with increasing heat treatment temperature. This result is also expected. The reported value of the oxidation potential of the P3HT HOMO level is -4.74 eV with respect to vacuum measured using cyclic voltametery[41] and ∼4.5 eV measured using ultraviolet photoelectron spectroscopy.[42, 43] As P3HT mixes with PSS the most easily removed electron comes from the HOMO of P3HT and so Φ of the surface is reduced. This change in the Φ shows that no vacuum level shift occurs at the interface between P3HT and PEDOT:PSS, as has been previously reported.[42]

The Φ measurements allow us to make several conclusions. First, the Φ of the mixed P3HT/PSS layer is set by the P3HT within the layer. Second, Φ is the same for mixtures of P3HT/PSS as for pure P3HT. Finally, since Φ is the same for 150°C, 180 °C, and 210°C P3HT washed samples, very little or extensive material mixing between P3HT and PSS does not

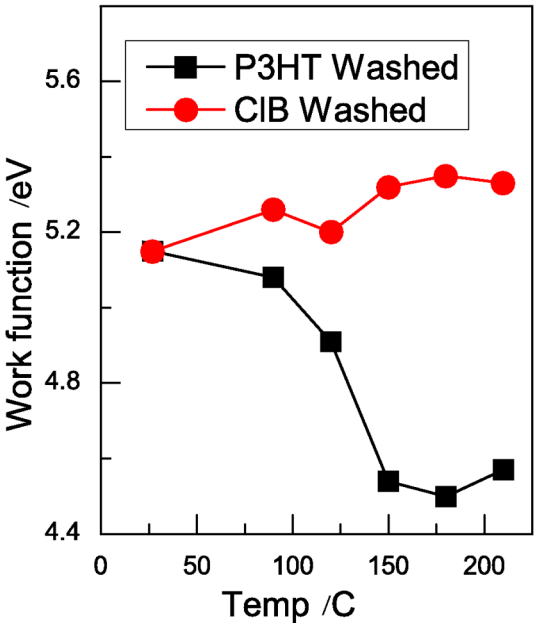

Figure 6: Work function measurements performed by Kelvin probe force microscopy of PEDOT:PSS layers that have or have not been coated with P3HT.

significantly change the work function.

PEDOT:PSS is known as a good hole conductor and hole only layer. The Kelvin force probe data indicates that the Fermi level is reduced at the interface to the BHJ layer which, in principle, reduces the total electric field across the BHJ layer and thereby the probability for separation of photogenerated electron-hole pairs.[44] However the presence of oxidized P3HT in the intermixed layer is highly selective for hole only transport, which should reduce the dark current and improve the fill factor (FF) of the OPV device. We have compared the temperature dependence of current-voltage (J–V) characteristics for devices cast from CB and CB/nitrobenzene (NB)[45] to separate the electronic effects due to BHJ morphology changes and mixed interface layer formation. The solvent additive NB has been shown to cause aggregation of the P3HT, which leads to an improved short-circuit current density (J_{sc}) and FF compared with as-cast devices that are solution cast from solvents such as CB and o-xylene. We have shown[46] that the NB additive does not evaporate out of the BHJ film, even upon heating to >150°C and that the presence of NB increases the onset of melting of the P3HT/PCBM blend by over 50°C. These results mean that, in effect, the morphology of bulk-heterojunction films with NB added does not change significantly upon heating. UV/Vis and fluorescence spectra of films heated to 180°C are identical to those of as-cast films, which shows that the morphology of the film is maintained by the presence of the NB.

Figure 7a shows J–V curves for P3HT:PCBM OPV devices cast from CB and CB/NB. The devices were measured directly after spin coating and after heating to 180°C. It can be seen that the J_{sc} and fill factor (FF) of the CB/NB-cast devices are nearly identical in the as-cast and heated devices, but that both of these characteristics increase greatly upon heating for the CB-cast device. We have already noted that the morphology of the CB/NB-cast devices does not change upon heating. The only clear change in the CB/NB J–V data is an increase of the V_{oc} from 0.6 V to 0.66 V. By comparison, the V_{oc} of the CB-cast device drops from 0.72 V to 0.66 V upon heating, as has been previously reported for increased order in P3HT.[47] Comparison of the two device types shows that the BHJ morphology controls the J_{sc} and FF while the V_{oc} also depends on the charge extraction potential at each electrode. Since the process of heating these devices causes the formation of a doped hole conducting interface, the V_{oc} also depends on the interface layer formation.

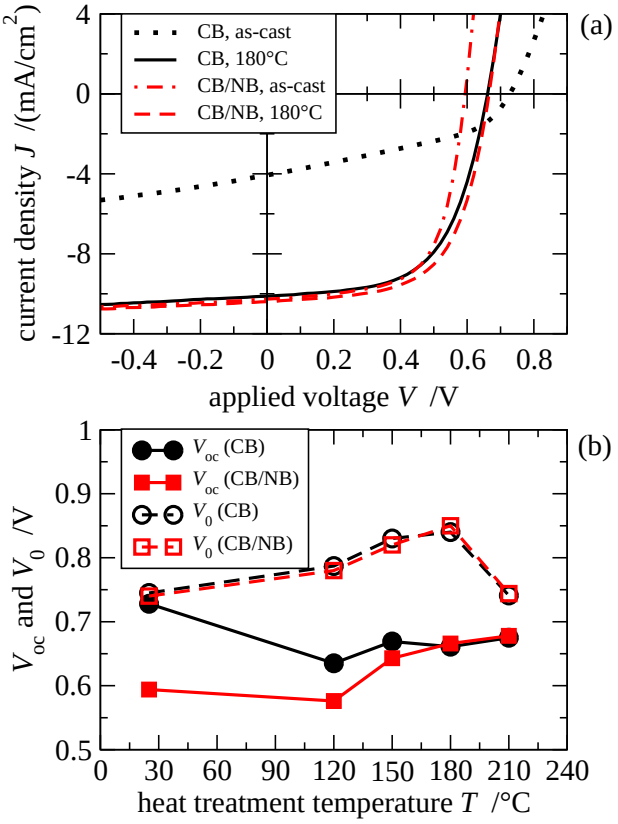

Figure 7: (a) Current–voltage curves of 3:2 w/w P3HT:PCBM devices spin cast from chlorobenzene (CB) and from chlorobenzene/nitrobenzene (CB/NB) that were as-cast or heat treated at 180°C. (b) V_{oc} and V_0 for devices cast from CB or CB/NB vs heat-treatment temperature.

Figure 7b shows a plot of V_{oc} versus heat-treatment temperature for a series of CB- and CB/NB-cast devices, in which it can be seen that V_{oc} for both device types varies non-monotonically. V_{oc} shows a minimum at 120°C and is the same for heat-

treatment temperatures above 180°C, but there is no obvious trend. A plot of the compensation voltage V_0 (the voltage at which the current–voltage curves in the dark and under illumination cross) versus heat-treatment temperature is also shown on the same axis. Heating the device up to temperatures of 180°C clearly increases V_0 for both device types. Interestingly, V_0 is nearly identical for both device types in Figure 7b as a function of the heat-treatment temperature. The value of V_0 in BHJ solar cells is the applied voltage required to compensate for the work function difference between the HOMO of the donor at the anode and the LUMO of the acceptor at the cathode.[48] Since the two device types have very different morphologies and very different *J–V* curves for most of these temperatures, we must conclude that something in addition to the bulk-heterojunction layer controls V_0. We recently reported that the onset of melting for P3HT samples with NB present is increased to over 180°C,[46] which indicates that for BHJ layers heated below 180°C the morphology with or without NB present is different. V_0 can be changed by the effects of band bending, formation of an interface dipole layer, or doping of the material at the interface. Correlation of the heat-treatment temperature dependence of the V_0 for both samples with the temperature dependence for the formation of P3HT/PSS interlayer (reported above) indicates that the increase in V_0 with increased heat treatmnt temperature is due to the formation of a PSS/P3HT interlayer with doped P3HT present. For a heat treatment temperature of 210°C the V_0 is reduced for both sample types. This is due to increased thickness of the interlayer that also increases the device series resistance. A separate detailed article that discusses the how morphology and mixed interface layer separately affect the current-voltage characteristics of OPV devices is in preparation.

The electrical properties of the device change because of the interlayer formation. HPSS and PSS are insulators. It can be assumed that the charge transport through the ∼3–7 nm thick interlayer occurs through the P3HT. Small-molecule OPV devices are fabricated with a donor/mixed/acceptor layer structure in order to increase the selectivity of charge transport to the two electrodes.[49] The increased compensation voltage V_0 with the formation of the interlayer, shown in Figure 7a, is indirect evidence of increased electrode selectivity for holes.

3 Conclusions

In conclusion, we have shown that heat treatment of P3HT/PCBM bulk-heterojunction layers that are deposited onto PEDOT:PSS hole transport layers leads to material mixing of the layers. Specifically, at temperatures at and above 150°C the P3HT forms an interlayer with PSS from the PEDOT:PSS. This mixed interlayer forms a 3-5 nm thick layer and is composed of a mixture of $P3HT^+$ and PSS^-. After formation, the mixed interlayer is insoluble to both organic solvents and to H_2O. The oxidized P3HT is the charge carrier, and since it is doped, it is very selective to hole transport. The work function of the mixed interlayer is nearly identical to the HOMO level of the P3HT, which indicates p-doping of the P3HT. Examination of the heat treatment temperature dependence of devices that were fabricated with differing morphologies shows that the formation of the mixed interlayer affects the open circuit voltage and increases the compensation voltage.

4 Experimental

Materials and Device Fabrication: All devices were fabricated on indium tin oxide (ITO) glass slides that had been etched with acid to a specified shape using a mask. The substrates were then cleaned in an ultrasonic bath with chloroform, acetone, mucasol, and deionized water. Prior to spin coating a ∼40 nm polyethylenedioxythiophene:polystyrenesulphonate (PEDOT:PSS; H.C. Starck) layer, the ITO substrates were placed in an ozone plasma for 30 min. The PEDOT:PSS-coated films were dried at 110°C for 3 min and then immediately taken into an N_2 glovebox. Mixtures of 3:2 w/w poly(3-hexylthiophene) (P3HT; Reike Metals):phenyl-C_{61}-butyric acid methyl ester (PCBM; Nano-C) were dissolved into chlorobenzene and then spin-coated onto the PEDOT:PSS surfaces to create film layers of 80 nm, as measured using a calibrated Dektak surface profilometer. For some of the devices, nitrobenzene was added to the spin-coating mixture directly before spin coating. Next, the samples were moved to a high vacuum chamber, where Ca/Ag electrodes were thermally evaporated through a shadow mask. All subsequent heating and measurement using the solar simulator were performed in the glovebox.

Samples for the washing experiments and reflectometry experiments were prepared on either cleaned glass slides or on silicon wafers with a native oxide layer. The cleaning steps were the same as described above. PEDOT:PSS was spin-coated on to the substrate followed by either P3HT or a mixture of P3HT and PCBM. The layered films were heated in the glovebox using a calibrated hot plate. The washing was performed by covering the entire film with chlorobenzene and then spinning the film. This process was repeated three to five times to ensure that any polymer not physically or chemically bound to the surface was washed away. Washing by soaking in an ultrasonic bath of chlorobenzene was also carried out, but gave the same contact angle results as those presented in this paper for the samples washed by spin-coating.

Device Measurements: AM1.5 light was provided by a filtered Xe lamp. The light intensity was calibrated using a Si photodiode but no mismatch factor was applied to the measurements. The *J–V* measurements were performed using a Keithley 2420 source measurement unit.

Contact Angle Measurements: Contact angle measurements were performed on a leveled goniometer stage. A droplet of H_2O was placed on the sample surface and then the contact an-

gle was measured using a height-adjusted microscope camera and angle-determination software.

XANES Measurements: X-ray absorption near edge structure (XANES) data were taken at beam line 4.0.2 of the Advanced Light Source synchrotron at the Lawrence Berkeley National Laboratory. The incident beam energy was scanned in increments of 0.5 eV in the energy range below the carbon K-edge from 250 to 275 eV, in 0.1 eV increments over the near-edge region from 275.1 to 300 eV, in increments of 0.2 eV from 300.2 to 330 eV and in increments of 0.5 eV in the featureless region from 330.5 to 360 eV. The slit settings were reduced to 20 μm / 20 μm and the incident beam was defocused to a spot size of roughly 1 mm^2 to avoid radiation damage to the film samples. The incident beam intensity I_0 was measured with a 95% transmissive gold grid after the refocusing mirror, and the total electron yield (TEY) was measured with a Photonis Channeltron Electron Multiplier (model CEM 4716). A custom-designed superconducting tunnel junction X-ray spectrometer[50] was used to simultaneously record the X-ray fluorescence from the sample for each incident energy, and the intensity of the carbon K line used as a measure of the partial fluorescence yield (PFY). Both TEY and PFY signals were normalized by I_0 and set to unity in the flat region of 350 to 360 eV above the absorption features. Offset voltages were carefully zeroed so that the spectra not contain any of the structure in I_0 due to a small carbon contamination of the monochromator.

Neutron Scattering Measurements: Neutron Reflectometry Measurements: The properties of the thin-film layers of samples of PEDOT:PSS and/or P3HT spin-coated onto silicon wafer substrates and subjected to various heat and solvent treatments were determined by neutron reflectometry. The neutron reflectometry measurements were carried out using the Surface Profile Analysis Reflectometer (SPEAR) at the Manuel Lujan Jr. Neutron Scattering Center at the Los Alamos National Laboratory. A collimated neutron beam was directed at a sample at an incident angle of θ. The reflectivity R, defined as the ratio of the intensity of the specularly reflected neutron beam to that of the incident beam, was measured as a function of the momentum change perpendicular to the surface, $Q_z = (4\pi \sin\theta)/\lambda$, also known as the momentum transfer vector. Here λ is the wavelength of the neutrons. The measured reflectivity was fit to a slab model, in which the sample film was assumed to consist of a series of n parallel layers, where layer i has a thickness d_i and constant scattering length density (SLD) ρ_i, sandwiched between super- (air) and subphases (silicon) of infinite extent. Interlayer "roughness" $\sigma_{i,i+1}$, which could include contributions from actual roughness between layers or from interlayer mixing, was accounted for by an error function SLD profile centered at the interface connecting the SLDs of the adjacent layers i and $(i+1)$. Model fitting to the measured data for $\log R$ vs Q_z was carried out with the Levenberg-Marquardt nonlinear least-squares method using the `MOTOFIT` program[51], in which the reflectivity profile is calculated using the Abeles matrix method[52]. The scattering length densities of air, the silicon substrate, and native oxide layer on the substrate were taken to be $\rho_{air} = 0$, $\rho_{Si} = 2.07 \times 10^{-6}$ Å^{-2}, and $\rho_{SiO_2} = 3.47 \times 10^{-6}$ Å^{-2}, respectively.[51] For simplicity, the roughnesses above the Si and SiO_2 layers were assumed to be zero.

Acknowledgements

This work was supported by the US Department of Energy EERE Solar America Initiative under Contract No. DE-FG36-08GO18018. The thank LANL for neutron reflectometry measurement time at the LANSCE-SPEAR facility and measurement help obtained from Erik Watkins and Jarek Majewski. We thank the ALS for providing beam time. Part of this work was performed under the auspices of the U.S. Department of Energy by Lawrence Livermore National Laboratory under Contract DE-AC52-07NA27344.

References

[1] M. Osborn, *New polymers push Solarmers OPV efficiency to record 8.13 percent*, www.pv-tech.org, **2010**.

[2] H. Hoppe, N. S. Sariciftci, *J. Mater. Chem.* **2006**, *16*, 45–61.

[3] G. Li, V. Shrotriya, Y. Yao, J. S. Huang, Y. Yang, *J. Mater. Chem.* **2007**, *17*, 3126–3140.

[4] A. J. Moulé, K. Meerholz, *Adv. Funct. Mater.* **2009**, *19*, 3028–3036.

[5] T. Erb, U. Zhokhavets, G. Gobsch, S. Raleva, B. Stuhn, P. Schilinsky, C. Waldauf, C. J. Brabec, *Adv. Funct. Mater.* **2005**, *15*, 1193–1196.

[6] V. D. Mihailetchi, H. X. Xie, B. de Boer, L. J. A. Koster, P. W. M. Blom, *Adv. Funct. Mater.* **2006**, *16*, 699–708.

[7] X. N. Yang, J. Loos, S. C. Veenstra, W. J. H. Verhees, M. M. Wienk, J. M. Kroon, M. A. J. Michels, R. A. J. Janssen, *Nano Lett.* **2005**, *5*, 579–583.

[8] G. Greczynski, T. Kugler, M. Keil, W. Osikowicz, M. Fahlman, W. R. Salaneck, *J. Elect. Spectros. Rel. Phenom.* **2001**, *121*, 1–17.

[9] S. Kirchmeyer, M. Reuter, *J. Mater. Chem.* **2005**, *15*, 2077–2088.

[10] A. M. Nardes, M. Kemerink, R. A. J. Janssen, J. A. M. Bastiaansen, N. M. M. Kiggen, B. M. W. Langeveld, A. van Breemen, M. M. de Kok, *Adv. Mater.* **2007**, *19*, 1196–1200.

[11] A. M. Nardes, M. Kemerink, R. A. J. Janssen, *Phys. Rev. B* **2007**, *76*, 085208–7.

[12] A. M. Nardes, M. Kemerink, M. M. de Kok, E. Vinken, K. Maturova, R. A. J. Janssen, *Org. Electron.* **2008**, *9*, 727–734.

[13] R. Steim, F. R. Kogler, C. J. Brabec, *Journal of Materials Chemistry* |**2010**|, *20*, 2499–2512.

[14] A. W. Hains, A. B. F. Liu, J. Martinson, M. D. Irwin, T. J. Marks, *J. Mater. Chem.* **2010**, *20*, 595–606.

[15] B. Maennig, J. Drechsel, D. Gebeyehu, P. Simon, F. Kozlowski, A. Werner, F. Li, S. Grundmann, S. Sonntag, M. Koch, K. Leo, M. Pfeiffer, H. Hoppe, D. Meissner, N. S. Sariciftci, I. Riedel, V. Dyakonov, J. Parisi, *Applied Physics a-Materials Science & Processing* **2004**, *79*, 1–14.

[16] K. Walzer, B. Maennig, M. Pfeiffer, K. Leo, *Chem. Rev.* **2007**, *107*, 1233–1271.

[17] G. Li, C. W. Chu, V. Shrotriya, J. Huang, Y. Yang, *Applied Physics Letters* **2006**, *88*, 253503.

[18] H. H. Liao, L. M. Chen, Z. Xu, G. Li, Y. Yang, *Applied Physics Letters* **2008**, *92*, 173303.

[19] M. D. Irwin, B. Buchholz, A. W. Hains, R. P. H. Chang, T. J. Marks, *Proceedings of the National Academy of Sciences of the United States of America* **2008**, *105*, 2783–2787.

[20] J. Hwang, F. Amy, A. Kahn, *Org. Electron.* **2006**, *7*, 387–396.

[21] Y. Kim, A. M. Ballantyne, J. Nelson, D. D. C. Bradley, *Org. Electron.* **2009**, *10*, 205–209.

[22] C. Tengstedt, W. Osikowicz, W. R. Salaneck, I. D. Parker, C. H. Hsu, M. Fahlman, *Appl. Phys. Lett.* **2006**, *88*, 053502.

[23] S. Braun, M. P. de Jong, W. Osikowicz, W. R. Salaneck, *Appl. Phys. Lett.* **2007**, *91*, 202108.

[24] M. C. Scharber, D. Wuhlbacher, M. Koppe, P. Denk, C. Waldauf, A. J. Heeger, C. L. Brabec, *Adv. Mater.* **2006**, *18*, 789–794.

[25] M. Gross, D. C. Muller, H. G. Nothofer, U. Scherf, D. Neher, C. Brauchle, K. Meerholz, *Nature* **2000**, *405*, 661–665.

[26] S. Bange, A. Kuksov, D. Neher, A. Vollmer, N. Koch, A. Ludemann, S. Heun, *Journal of Applied Physics* **2008**, *104*, 104506.

[27] F. Zhang, A. Vollmer, J. Zhang, Z. Xu, J. P. Rabe, N. Koch, *Organic Electronics* **2007**, *8*, 606–614.

[28] G. Heimel, I. Salzmann, S. Duhm, J. P. Rabe, N. Koch, *Advanced Functional Materials* **2009**, *19*, 3874–3879.

[29] J.-S. Kim, R. H. Friend, I. Grizzi, J. H. Burroughes, *Appl. Phys. Lett.* **2005**, *87*, 023506.

[30] A. B. D. Cassie, S. Baxter, *Trans. Faraday Soc.* **1944**, *40*, 546–551.

[31] D. Schmeisser, M. Tallarida, K. Henkel, K. Müller, D. Mandal, D. Chumakov, E. Zschech, *Mater. Sci. Pol.* **2009**, *27*, 141–157.

[32] S. K. M. Jonsson, M. P. de Jong, L. Groenendaal, W. R. Salaneck, M. Fahlman, *J. Phys. Chem. B* **2003**, *107*, 10793–10800.

[33] National Institute of Standards and Technology (NIST) Center for Neutron Research, Scattering Length Density Calculator: http://www.ncnr.nist.gov/resources/sldcalc.html.

[34] K. Peter, C. Volhardt, N. E. Schore, *Organic Chemistry: Structure and Function*, Freeman and Co., **2003**.

[35] M. M. Bouman, E. E. Havinga, R. A. J. Janssen, E. W. Meijer, *Molecular Crystals and Liquid Crystals Science and Technology Section a-Molecular Crystals and Liquid Crystals* **1994**, *256*, 439–448.

[36] R. Osterbacka, C. P. An, X. M. Jiang, Z. V. Vardeny, *Science* **2000**, *287*, 839–842.

[37] K. H. Yim, G. L. Whiting, C. E. Murphy, J. J. M. Halls, J. H. Burroughes, J. S. Kim, *Adv. Mater.* **2008**, *20*, 3319–3324.

[38] C. Y. Kao, B. Lee, L. S. Wielunski, M. Heeney, I. McCulloch, E. Garfunkel, L. C. Feldman, V. Podzorov, *Advanced Functional Materials* **2009**, *19*, 1906–1911.

[39] O. Tal, W. Gao, C. K. Chan, A. Kahn, Y. Rosenwaks, *Appl. Phys. Lett.* **2004**, *85*, 4148–4150.

[40] D. Cahen, A. Kahn, *Adv. Mater.* **2003**, *15*, 271–277.

[41] P. Zacharias, M. C. Gather, M. Rojahn, O. Nuyken, K. Meerholz, *Angew. Chem. Int. Ed.* **2007**, *46*, 4388–4392.

[42] M. Fahlman, A. Crispin, X. Crispin, S. K. M. Henze, M. P. d. Jong, W. Osikowicz, C. Tengstedt, W. R. Salaneck, *J. Phys.: Condens. Matter* **2007**, 183202.

[43] S. Braun, W. R. Salaneck, M. Fahlman, *Adv. Mater.* **2009**, *21*, 1450–1472.

[44] L. J. A. Koster, E. C. P. Smits, V. D. Mihailetchi, P. W. M. Blom, *Physical Review B* **2005**, *72*, 085205.

[45] A. J. Moulé, K. Meerholz, *Adv. Mater.* **2008**, *20*, 240–245.

[46] L. Chang, H. W. A. Lademann, J. Bonekamp, K. Meerholz, A. J. MouleÃŇÂĄ, *Adv. Funct. Mater. (In Press)* **2011**.

[47] M. Campoy-Quiles, Y. Kanai, A. El-Basaty, H. Sakai, H. Murata, *Organic Electronics* **2009**, *10*, 1120–1132.

[48] V. D. Mihailetchi, L. J. A. Koster, J. C. Hummelen, P. W. M. Blom, *Phys. Rev. Lett.* **2004**, *93*, 216601.

[49] P. Peumans, S. Uchida, S. R. Forrest, *Nature* **2003**, *425*, 158–162.

[50] S. Friedrich, O. B. Drury, S. J. George, S. P. Cramer, *Nuc. Inst. & Meth. Phys. Res.* **2007**, *582*, 187–189.

[51] A. Nelson, *J. Appl. Cryst.* **2006**, *39*, 273–276.

[52] O. S. Heavens, *Optical Properties of Thin Solid Film*, Dover, New York, **1991**.

Supporting Information for “The Consequences of Interface Mixing on Organic Photovoltaic Device Characteristics”

David M. Huang, Scott A. Mauger, Stephan Friedrich,
Simon J. George, Daniela Dimitriu LaGrange, Sook Yoon, and Adam J. Moulé

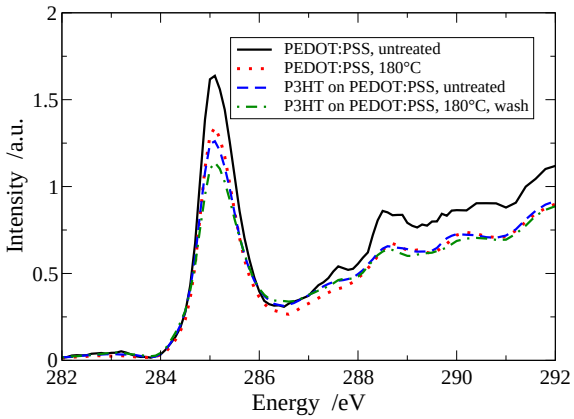

Figure S1: X-ray absorption near edge structure (XANES) spectra of the carbon K edge of untreated PEDOT:PSS (solid line), PEDOT:PSS heated to 180°C (dotted line), untreated P3HT on PEDOT:PSS (dashed line). and P3HT on PEDOT:PSS that was heated to 180°C and then washed with chlorobenzene (dot-dashed line).

References

[1] T. A. Chen, X. M. Wu, R. D. Rieke, *Journal of the American Chemical Society* **1995**, *117*, 233–244.

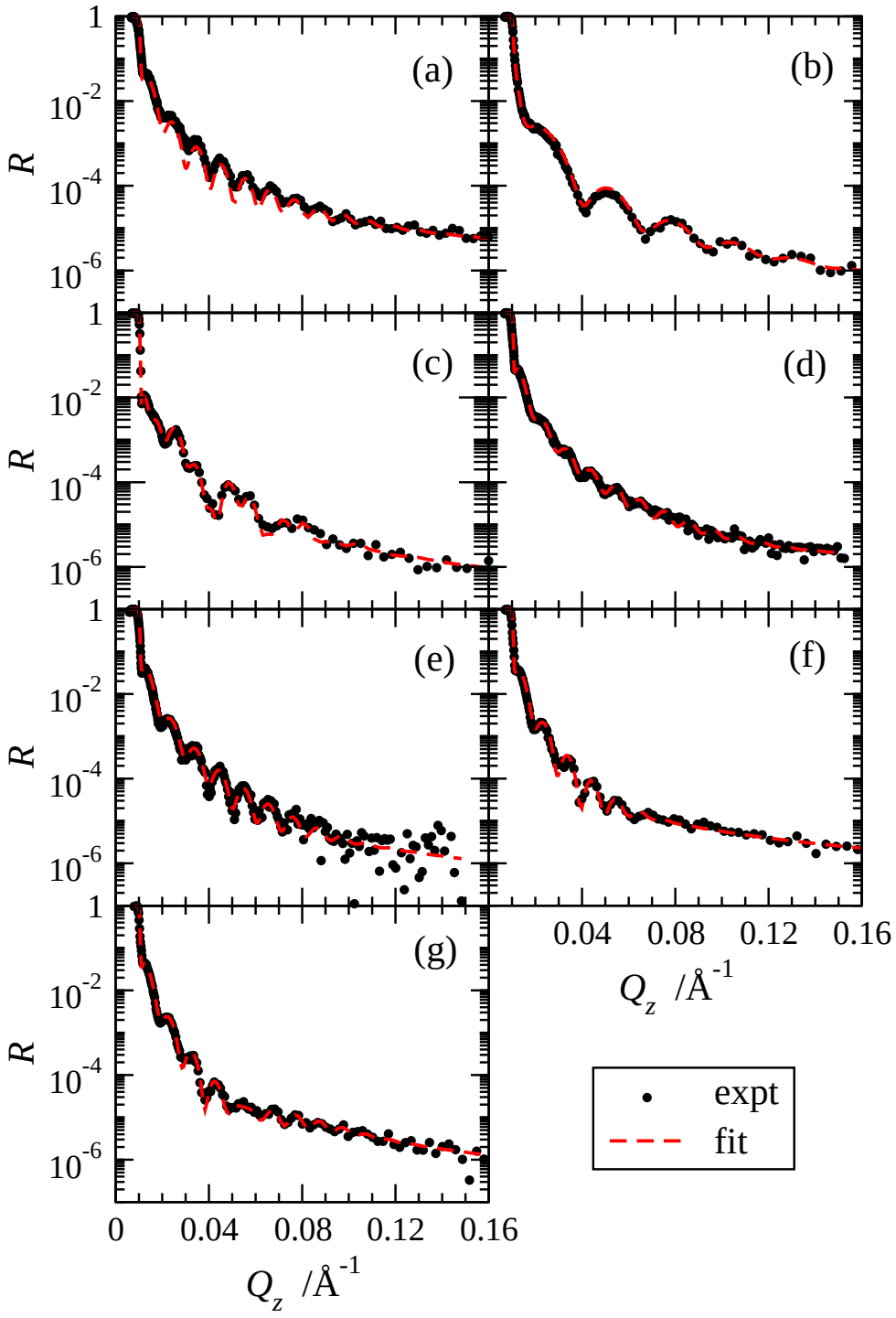

Figure S2: Reflectivity R vs momentum transfer vector Q_z from measurements (points) and fits (lines) of various samples on silicon wafers: (a) PEDOT:PSS, (b) P3HT, (c) unwashed P3HT on PEDOT:PSS, and P3HT on PEDOT:PSS heated then washed with chlorobenzene, with heat treatment temperature of (d) room temperature, (e) 150°C, (f) 180°C, and (g) 210°C.

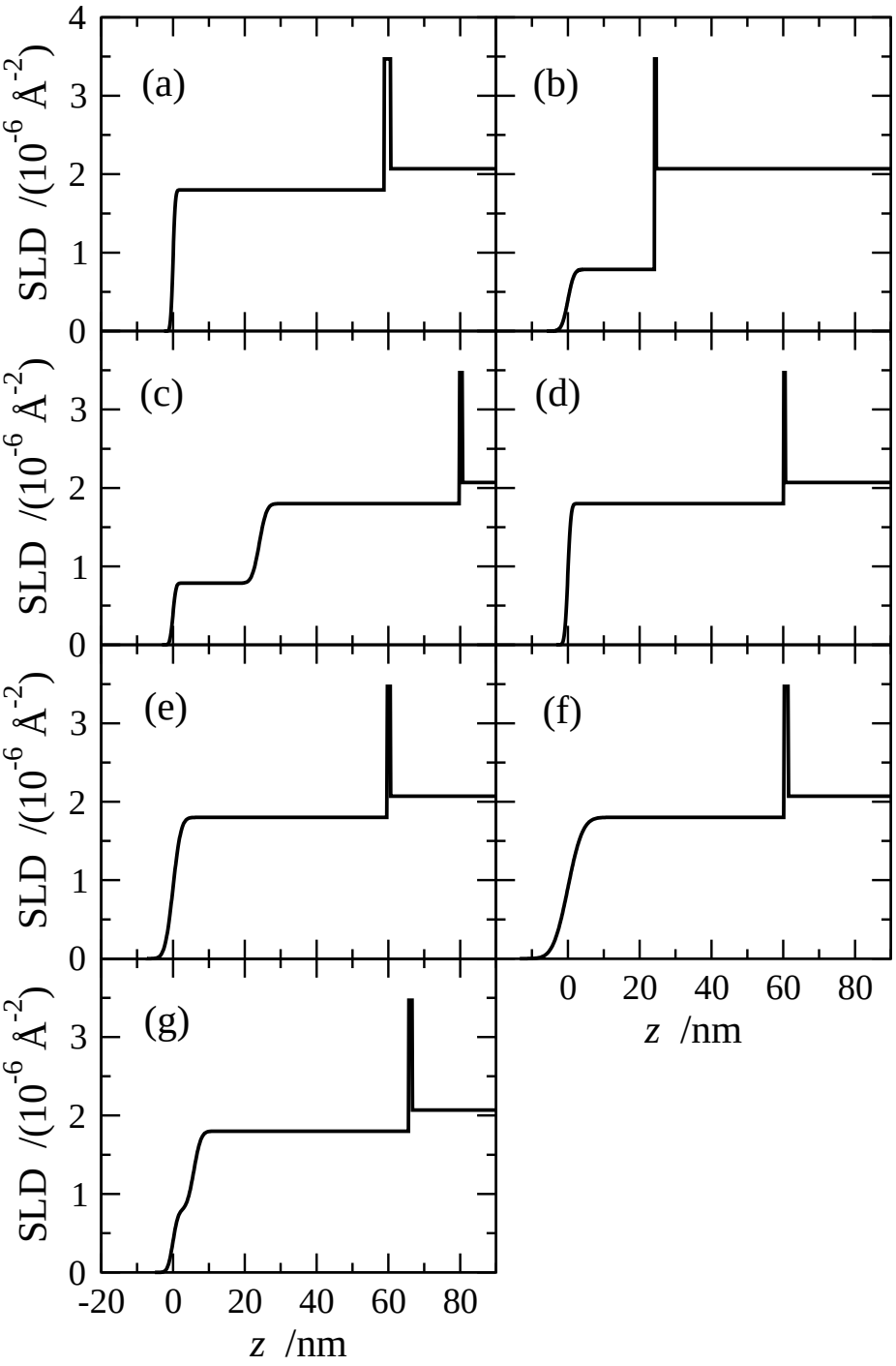

Figure S3: Scattering length density SLD vs distance from the top surface of samples from fits to the measured reflectivity data in Figure S2: (a) PEDOT:PSS, (b) P3HT, (c) unwashed P3HT on PEDOT:PSS, and P3HT on PEDOT:PSS heated then washed with chlorobenzene, with heat treatment temperature of (d) room temperature, (e) 150°C, (f) 180°C, and (g) 210°C.

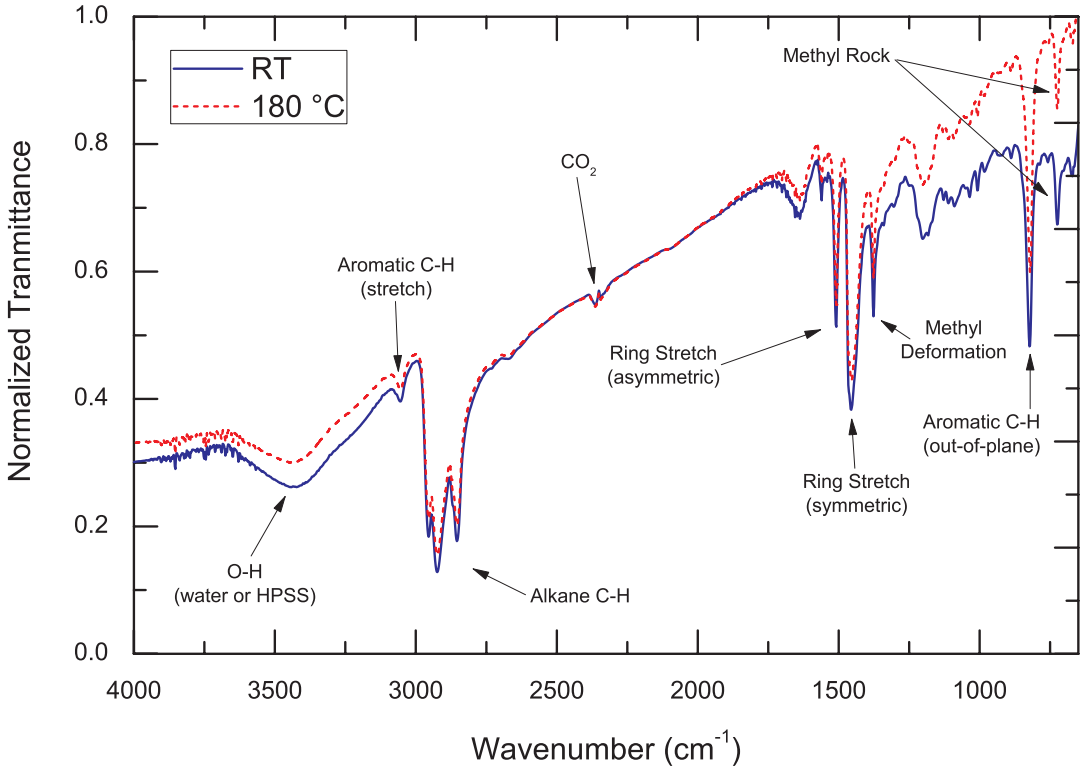

Figure S4: FTIR spectra of mixed P3HT/PEDOT:PSS before (line) and after (dotted line) heat treatment at 180°C. The P3HT and dried PEDOT:PSS were mixed as powder samples in a mortar and pestle with KBr. Half of the samples was subsequently heated to 180°C. Then both samples were mechanically pressed and measured in transmission in the FTIR. The differences in the spectra come from sample geometry. There is no evidence of new peak formation or a change in the peak ratios. Assignments of the peaks were taken from Chen et. al.[1]

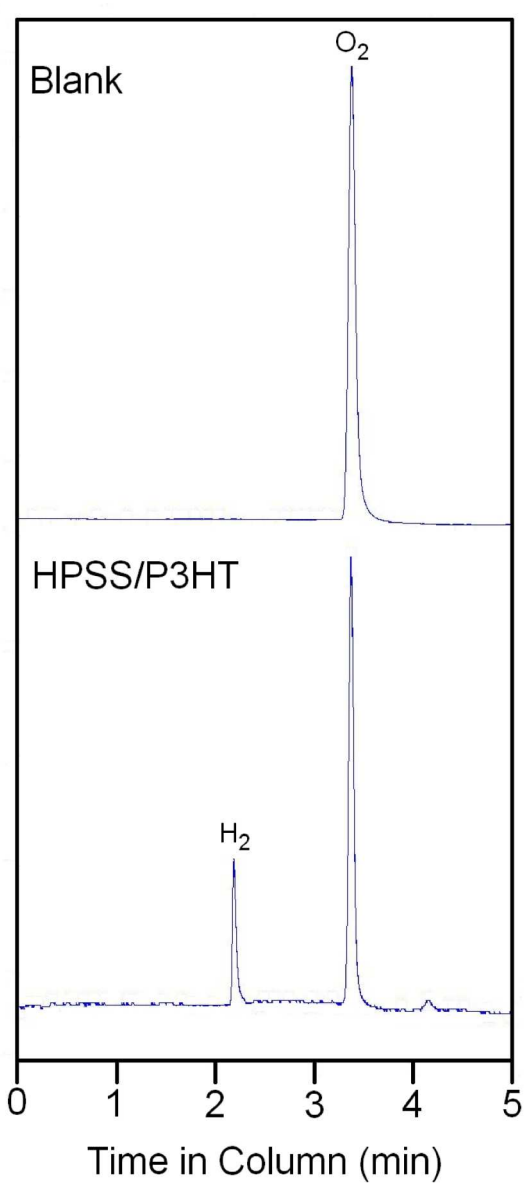

Figure S5: Gas chromatograph mass spectometry of a gaseous sample taken from a vial with a mixture of HPSS and P3HT that had left at room temperature (upper) and that had been heated to 180°C for 10 min. The vial that had been heated has a H_2 peak, indicating that the proposed mechansim is correct.